

Ferromagnetic Mott state in Twisted Graphene Bilayers at the Magic Angle

Kangjun Seo,¹ Valeri N. Kotov,² and Bruno Uchoa^{1,*}

¹*Department of Physics and Astronomy, University of Oklahoma, Norman, Oklahoma 73069, USA*

²*Department of Physics, University of Vermont, Burlington, Vermont 05405, USA*



(Received 6 December 2018; published 18 June 2019)

We address the effective tight-binding Hamiltonian that describes the insulating Mott state of twisted graphene bilayers at a magic angle. In that configuration, twisted bilayers form a honeycomb superlattice of localized states, characterized by the appearance of flat bands with fourfold degeneracy. After calculating the maximally localized superlattice Wannier wave functions, we derive the effective spin model that describes the Mott state. We suggest that the system is an exotic *ferromagnetic* Mott insulator, with well-defined experimental signatures.

DOI: 10.1103/PhysRevLett.122.246402

Introduction.—Mott insulators describe materials that exhibit insulating behavior as a result of strong local interactions [1]. In those systems, strong on site repulsion penalizes the kinetic energy for electrons to hop between sites, rendering the electronic orbitals localized. The strong degree of localization of the electronic wave functions favors antiferromagnetic alignment of the spins due to Pauli principle [2]. Recent experiments [3,4] indicate that twisted graphene bilayers have a Mott state with an activation gap of $\Delta \approx 0.3$ meV that undergoes a metal-insulator transition in the vicinity of a superconducting phase [4,5]. This system is purely made of carbon atoms, with additional degrees of freedom inherited from graphene [6]. That has motivated the question of whether the observed state could be described by a novel Mott insulator [7] or other exotic correlated states [8–12]. Unveiling the nature of the insulating state may be key to explaining some of the remarkable properties in the metallic phase.

By twisting two graphene sheets at a small angle of the order of $\theta \sim 1.1^\circ$, what was dubbed a “magic” angle, interference due to hopping between the layers leads to a moiré pattern and to a significant reconstruction of the mini bands in the moiré Brillouin zone, which become flat [13,14]. Those flat bands have fourfold degeneracy, which is reminiscent of the valley and spin quantum numbers of the graphene sheets. In general, the confinement of interacting Dirac fermions in flat bands is expected to create an emergent $SU(4)$ symmetry, as previously predicted in graphene heterostructures [15–17] and in graphene Landau levels [18–24]. Here, the moiré pattern forms a superlattice of quasilocized states with the size of the unit cell set by the twist angle, as shown in Fig. 1.

In this Letter, we show that the low energy Hamiltonian of the flat bands at quarter filling maps into the *ferromagnetic* spin exchange Hamiltonian on a honeycomb superlattice,

$$\mathcal{H} = - \sum_{ij} J_{ij} \left(\frac{1}{2} + 2\tau_i^z \tau_j^z - 2\eta_{ij} \tau_i^\perp \cdot \tau_j^\perp \right) \left(\frac{1}{2} + 2\mathbf{S}_i \cdot \mathbf{S}_j \right), \quad (1)$$

where \mathbf{S}_i is the localized spin on a superlattice site i , $\boldsymbol{\tau}_i = (\tau_i^x, \tau_i^y, \tau_i^z) \equiv (\boldsymbol{\tau}_i^\perp, \tau_i^z)$ is an orbital pseudospin operator that is reminiscent of the valley quantum numbers, and $J_{ij} > 0$ is the exchange coupling. The parameter $\eta_{ij} = -1$ when i, j belong to the same sublattice, in which case the exchange interaction has $SU(4)$ symmetry, and $\eta_{ij} = 1$ otherwise, including nearest neighbor (NN) sites. This Hamiltonian acts in the Hilbert space, which is spanned by four degenerate states per site, $|\alpha, \sigma\rangle$, with $\alpha = \pm$ and $\sigma = \uparrow, \downarrow$ for the two orbital pseudospins and spin quantum numbers, respectively.

The existence of direct exchange ferromagnetism in an insulating state is uncommon [15] and reflects the very

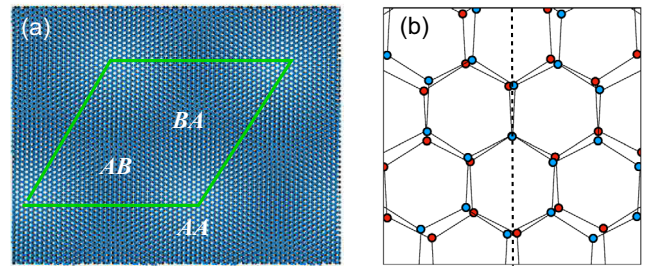


FIG. 1. (a) Moiré pattern of twisted graphene bilayers for a twist angle of $\theta = 1.8^\circ$. Each layer has two sublattices, A and B. The pattern indicates regions of AA, AB, and BA alignment. Fourfold degenerate states are observed around the AA stacking regions. (b) Twisted graphene bilayer rotated around A sites (AA region). At those points, the bilayer has D_3 symmetry, comprised of a C_3 rotation around the z axis and a C_2' rotation around the y axis (dashed line) in between two layers. Red and blue dots: top and bottom layer.

unusual shape of the Wannier orbitals in this system. Ferromagnetism has been recently observed in insulating van der Waals heterostructures of magnetic chromium trihalide materials, Cr X_3 ($X = \text{I, Br, Cl}$) [25–27], which have crystalline field anisotropies that produce an ordered Ising state. To the best of our knowledge, we are not aware of any examples of ferromagnetic Mott states that do not involve orbital ordering via a superexchange mechanism [28,29].

After performing calculations of the maximally localized Wannier orbitals of the moiré superstructure, we establish the parameters of a *minimal* interacting tight-binding model that captures the Mott physics near the magic angle. We show that even though the orbitals are well localized in the Mott regime at a quarter filling, surprisingly the direct *exchange* interaction between different sites is dominant and favors ferromagnetic spin order at zero temperature. While charging effects [30,31], which were not taken into account, may change our conclusions, the scenario of zero temperature ferromagnetism in twisted graphene bilayers seems in line with the reduced degeneracy of the Landau levels measured with Shubnikov–de Haas experiments near quarter filling [3]. We discuss the experimental signatures of this state.

Bloch Hamiltonian.—The free Hamiltonian for twisted graphene bilayers can be constructed at the lattice level using a parametrization for the hopping amplitudes between sites in the two different sheets,

$$\mathcal{H} = \begin{pmatrix} \mathcal{H}_g^{(1)} & \mathcal{H}_\perp \\ \mathcal{H}_\perp^\dagger & \mathcal{H}_g^{(2)} \end{pmatrix}, \quad (2)$$

where \mathcal{H}_g is the graphene Hamiltonian and \mathcal{H}_\perp is the interlayer hopping between the two sheets in real space. The moiré pattern can be used to construct Bloch states that are periodic in the superlattice vectors \mathbf{T}_i . For commensurate structures, the moiré lattice vectors are parametrized by two integers m and r , and correspond to the twist angle $\cos \theta = 1 - r^2/2(3m^2 + 3mr + r^2)$, or equivalently $\theta \approx r/\sqrt{3}m$ for small angles.

In a basis for Bloch states

$$\Phi_{\mathbf{k},\sigma} \equiv (|\varphi_{\mathbf{k},A,\sigma}^{(1)}\rangle, |\varphi_{\mathbf{k},B,\sigma}^{(1)}\rangle, |\varphi_{\mathbf{k},A,\sigma}^{(2)}\rangle, |\varphi_{\mathbf{k},B,\sigma}^{(2)}\rangle), \quad (3)$$

defined in the two sublattices A and B of each of the two layers (1,2), the Bloch Hamiltonian of the twisted system

$$\mathcal{H}_{\mathbf{k}}(\mathbf{r}, \mathbf{r}') = \sum_i \mathcal{H}(\mathbf{r}, \mathbf{r}' + \mathbf{T}_i) e^{i\mathbf{k} \cdot \mathbf{T}_i} \quad (4)$$

satisfies $\mathcal{H}_{\mathbf{k}}(\mathbf{r}, \mathbf{r}' + \mathbf{T}_i) = \mathcal{H}_{\mathbf{k}}(\mathbf{r}, \mathbf{r}') e^{-i\mathbf{k} \cdot \mathbf{T}_i}$. In that basis,

$$[\mathcal{H}_{\mathbf{k}}]_{ab} = t_{\mathbf{k}}^{ab}(\mathbf{r}, \mathbf{r}') = \sum_j e^{i\mathbf{k} \cdot \mathbf{T}_j} t^{ab}(\mathbf{r}, \mathbf{r}' + \mathbf{T}_j) \quad (5)$$

are the matrix elements of Eq. (2), with a, b indexes running over the four components of basis [Eq. (3)]. The hopping amplitudes $t^{ab}(\mathbf{r}, \mathbf{r}') = \cos^2 \theta_z V_\sigma(\mathbf{r} - \mathbf{r}') + \sin^2 \theta V_\pi(\mathbf{r} - \mathbf{r}')$, where $\cos \theta_z = d/\sqrt{d^2 + (\mathbf{r} - \mathbf{r}')^2}$ with d being the distance between the planes. $V_\sigma(\mathbf{r})$ and $V_\pi(\mathbf{r})$ are Slater-Koster functions [32], which decay exponentially and were parameterized following previous *ab initio* works [33,34].

Diagonalization of the Bloch Hamiltonian results in a set of four-component Bloch eigenspinors $\hat{\psi}_{n,\mathbf{k}}(\mathbf{r}) \equiv \langle \mathbf{r} | \hat{\psi}_{n,\mathbf{k}} \rangle$ that satisfy $\hat{\psi}_{n,\mathbf{k}}(\mathbf{r} + \mathbf{T}) = \hat{\psi}_{n,\mathbf{k}}(\mathbf{r}) e^{i\mathbf{k} \cdot \mathbf{T}}$ and correspond to the energy spectrum $\varepsilon_n(\mathbf{k})$. We calculate the bands for a small twist angle of $\theta = 1.0845^\circ$ ($m = 30, r = 1$) near the experimental magic angle $\theta_0 \sim 1.1^\circ$. At that angle, the Bloch Hamiltonian is a $N_s \times N_s$ matrix with $N_s = 11164$ sites inside the moiré unit cell. The low energy bands ($n = 1, \dots, 4$), shown in Fig. 2(b), are fourfold degenerate at the K points (excluding the spin). They have a twofold degeneracy at the other two high symmetry points of the Brillouin zone, Γ' and M' , where they open up a gap between particle and hole branches. At the Γ' point, the Bloch states have C_3 and C_{2y} symmetry, which involves a π rotation around the y axis placed halfway between the two layers [shown in Fig. 1(b)]. We also find numerically that all Bloch eigenspinors satisfy the time reversal symmetry (TRS) relation $\mathcal{T} \hat{\psi}_{n,\mathbf{k}}(\mathbf{r}) = \hat{\psi}_{n,-\mathbf{k}}^*(\mathbf{r})$, with \mathbf{k} measured from the center of the moiré Brillouin zone at Γ' . The K and K' points are hence related by TRS, and must have opposite π Berry phases. This fact indicates that the Bloch states of the twisted structure do not suffer from Wannier obstructions [35], and hence could be reconstructed through a proper basis of Wannier states.

Wannier orbitals.—From the Bloch states of the four low energy bands, one can extract the Wannier wave functions in the moiré unit cell,

$$|\mathbf{R}\nu\rangle = \frac{1}{N_s} \sum_{n,\mathbf{k}} e^{-i\mathbf{k} \cdot \mathbf{R}} U_{n\nu}(\mathbf{k}) |\hat{\psi}_{n,\mathbf{k}}\rangle, \quad (6)$$

where \mathbf{R} is the center of the Wannier orbitals and $U_{n\nu}(\mathbf{k})$ some 4×4 unitary transformation. The four component

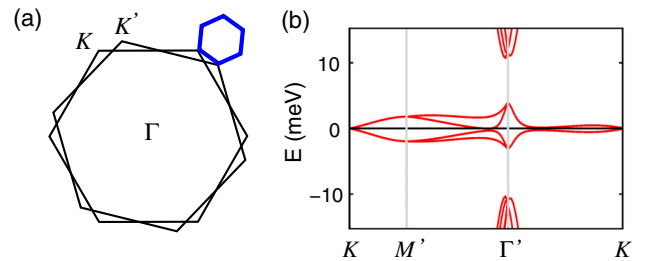


FIG. 2. (a) Moiré Brillouin zone of the twisted graphene system (blue hexagon), containing the K and K' points at the corners. (b) Flat bands in the moiré Brillouin zone for $\theta = 1.0845^\circ$, near the magic angle $\theta_0 \sim 1.1^\circ$. The Γ' point is at the center of the Moiré Brillouin zone. M' is the midpoint between K and K' points.

Wannier spinors $\hat{W}_\nu(\mathbf{r} - \mathbf{R}) \equiv \langle \mathbf{r} | \mathbf{R} \nu \rangle$ are not unique since adding a phase to the Bloch state $e^{-i\mathbf{k} \cdot \mathbf{r}} \hat{\psi}_{n\mathbf{k}}(\mathbf{r})$ corresponds to a new set of Wannier orbitals. We choose the set of maximally localized Wannier orbitals in finding the unitary transformation that minimizes their spread, $\Omega = \sum_\nu [\langle r^2 \rangle_\nu - \langle \mathbf{r} \rangle_\nu^2]$, with $\langle X \rangle_\nu \equiv \langle \mathbf{R} \nu | X | \mathbf{R} \nu \rangle$. The minimization was carried with the WANNIER90 package [36]. The momentum space \mathbf{k} mesh points are generated by the reciprocal supercell lattice vectors with 300×300 grid points using periodic boundary conditions, including all high symmetry points.

Following the symmetry arguments outlined in Ref. [37], we perform the minimization of the spread enforcing the C_3 and C'_{2y} symmetry for the Bloch states around the Γ' points. Those two symmetries describe a D_3 point symmetry group, which is a local symmetry of the lattice at AA site regions when the two graphene layers are rotated around a site [38], as depicted in Fig. 1(b). In agreement with earlier results [37,39], the Wannier functions that satisfy those symmetries have three sharp peaks centered around either the AB or BA sites, forming a honeycomb superlattice with twofold degenerate orbitals per site, as shown in Fig. 3.

On a given moiré unit cell, we label the Wannier orbitals by the four-component spinors $\hat{W}_\nu = (w_{\nu,1}, w_{\nu,2}, w_{\nu,3}, w_{\nu,4})^T$. Among the four orbitals, $\hat{W}_\nu(\mathbf{r} - \mathbf{R}_j)$, two are centered at $R_j \in AB$ sites and are eigenstates of the C_3 rotation operator, with eigenvalues $\epsilon = e^{2\pi i/3}$ and ϵ^* . The other two are centered at $R_j \in BA$ sites and also have the same eigenvalues ϵ and ϵ^* . From now on, we will label the Wannier orbital spinors based on their C_3 rotation eigenvalues, $C_3 \hat{W}_\alpha(\mathbf{r} - \mathbf{R}_j) = e^{i2\pi/3} \hat{W}_\alpha(\mathbf{r} - \mathbf{R}_j)$, with $\alpha = \pm$ and $R_j \in AB$ or BA . The two degenerate orbitals centered at a given superlattice site \mathbf{R}_j are related by TRS,

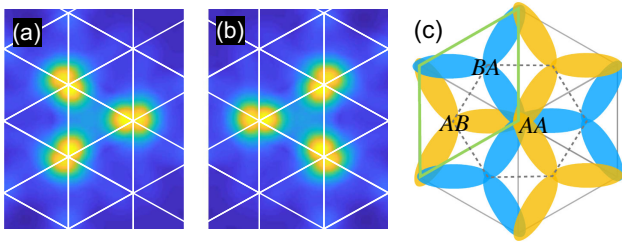


FIG. 3. Wannier wave function in the moiré superlattice. Amplitude $|\hat{W}_+(\mathbf{r} - \mathbf{R}_j)| = |\hat{W}_-(\mathbf{r} - \mathbf{R}_j)|$ of the orbitals centered around (a) $j \in AB$ sites, and (b) $j \in BA$ sites, showing three sharp peaks. The orbitals \hat{W}_α have twofold degeneracy per site, and are eigenstates of the C_3 rotation operator with eigenvalues ϵ ($\alpha = +$), and ϵ^* ($\alpha = -$). (c) Sketch of the orbitals in the moiré unit cell (green line). Orange: AB centered Wannier orbitals. Blue: BA centered ones. The gray dotted line indicates the honeycomb superlattice formed by the center of the orbitals. Their unusual three peak structure indicates strong overlap between superlattice sites, favoring ferromagnetic ordering at zero temperature.

$\mathcal{T} \hat{W}_\alpha(\mathbf{r} - \mathbf{R}_j) = \hat{W}_{-\alpha}(\mathbf{r} - \mathbf{R}_j)$. Orbitals in NN superlattice sites \mathbf{R}_i and \mathbf{R}_j are related by the C'_2 rotation, $C'_2 \hat{W}_\alpha(\mathbf{r} - \mathbf{R}_i) = \hat{W}_{-\alpha}(\mathbf{r} - \mathbf{R}_j)$.

Tight binding Hamiltonian.—The effective lattice model of this problem can be constructed by rewriting the Bloch Hamiltonian [Eq. (4)] into a kinetic energy term of the form

$$\mathcal{H} = \sum_{i,j} t_{\alpha\beta}(\mathbf{R}_{ij}) d_{\alpha,\sigma}^\dagger(\mathbf{R}_i) d_{\beta,\sigma}(\mathbf{R}_j), \quad (7)$$

where \mathbf{R}_i indexes the sites of the honeycomb superlattice, $\mathbf{R}_{ij} \equiv \mathbf{R}_i - \mathbf{R}_j$ and the $d_\alpha(\mathbf{R})$ annihilates an electron with orbital of type α and spin σ at a given superlattice site. The hopping matrix elements between superlattice sites can be extracted from the matrix elements of the Hamiltonian [Eq. (2)] in a basis of maximally localized Wannier functions,

$$t_{\alpha\beta}(\mathbf{R}_i) = \langle \mathbf{R} \alpha | \mathcal{H} | \mathbf{R} + \mathbf{R}_i, \beta \rangle. \quad (8)$$

Due to the translational invariance of the superlattice, $t_{\alpha\beta}(\mathbf{R}) = \langle 0, \alpha | \mathcal{H} | \mathbf{R}, \beta \rangle$. For NN sites, we find that $|t_{\alpha\alpha}|(1) \approx 0.384$ meV whereas for n th NN sites $t_{\alpha,-\alpha}(n) = 0$. Hence, hopping between sites conserves the orbital pseudospin quantum number $\alpha = \pm$. $|t_{\alpha\alpha}|(n)$ has a nontrivial dependence with the distance between sites (see Table I), in qualitative agreement with the findings of Ref. [37] for a significantly larger twist angle.

The Coulomb interactions between lattice sites can be written as $\mathcal{H}_C = \frac{1}{2} \int d\mathbf{r} d\mathbf{r}' \rho(\mathbf{r}) [e^2 / (\kappa |\mathbf{r} - \mathbf{r}'|)] \rho(\mathbf{r}')$, where $\rho(\mathbf{r})$ is the electron density and $\kappa \approx 5$ the dielectric constant of twisted bilayers encapsulated in boron nitride. We can rewrite this term in terms of $d_{\alpha,\sigma}$ operators by expressing the density $\rho(\mathbf{r}) = \sum_\sigma \hat{\Psi}_\sigma^\dagger(\mathbf{r}) \hat{\Psi}_\sigma(\mathbf{r})$ in terms of field operators $\hat{\Psi}_\sigma(\mathbf{r}) = \sum_{\alpha,j} \hat{W}_\alpha(\mathbf{r} - \mathbf{R}_j) d_{\alpha,\sigma}(\mathbf{R}_j)$. The resulting Coulomb Hamiltonian has a direct term and also an exchange part, $\mathcal{H}_C = \mathcal{H}_d + \mathcal{H}_e$. The first term,

$$\mathcal{H}_d = \sum_{i,j} V_{\alpha\beta}(\mathbf{R}_{ij}) n_\alpha(\mathbf{R}_i) n_\beta(\mathbf{R}_j), \quad (9)$$

with $n_\alpha(\mathbf{R}) = \sum_\sigma d_{\alpha,\sigma}^\dagger(\mathbf{R}) d_{\alpha,\sigma}(\mathbf{R})$ the density operator and repeated α, β indexes to be summed. The Coulomb coupling is cast as an overlap integral of Wannier orbital spinors, $V_{\alpha\beta}(\mathbf{R}_{ij}) = \frac{1}{2} \int d\mathbf{r} d\mathbf{r}' |\hat{W}_\alpha(\mathbf{r}_i)|^2 [e^2 / (\kappa |\mathbf{r} - \mathbf{r}'|)] |\hat{W}_\beta(\mathbf{r}_j)|^2$, with $\mathbf{R}_{ij} = \mathbf{R}_i - \mathbf{R}_j$ and $\mathbf{r}_j \equiv \mathbf{r} - \mathbf{R}_j$. The exchange part is

$$\mathcal{H}_e = \sum_{i \neq j} J_{\alpha\alpha',\beta\beta'}(\mathbf{R}_{ij}) d_{\alpha,\sigma}^\dagger(\mathbf{R}_i) d_{\beta,\sigma'}^\dagger(\mathbf{R}_j) d_{\beta',\sigma'}(\mathbf{R}_i) d_{\alpha',\sigma}(\mathbf{R}_j), \quad (10)$$

where the coupling $J_{\alpha\alpha',\beta\beta'}(\mathbf{R}_{ij}) = \frac{1}{2} \int d\mathbf{r} d\mathbf{r}' \hat{W}_\alpha^\dagger(\mathbf{r}_i) \hat{W}_{\alpha'}(\mathbf{r}_j) [e^2 / (\kappa |\mathbf{r} - \mathbf{r}'|)] \hat{W}_\beta^\dagger(\mathbf{r}_j) \hat{W}_{\beta'}(\mathbf{r}_i)$ is the exchange integral between lattice sites. In general, we find that the combinations $J_{\alpha\beta,\beta\alpha}(\mathbf{R}_{ij}) = J_{\alpha\beta,\alpha\beta}(\mathbf{R}_{ij}) = 0$ for $\alpha \neq \beta$, within the

TABLE I. Electronic hopping amplitude $|t_{\alpha\beta}|$, direct Coulomb interaction $V_{\alpha\beta}$ and exchange interaction $J_{\alpha\beta}$ for various nearest neighbor sites: on site (0), and n th nearest neighbors (n), with $n = 1-6$. Energies in meV calculated for $\kappa = 5$. $n = 1, 3$, and 4 correspond to sites in opposite sublattices. $J_{\alpha\alpha} \approx \pm J_{\alpha,-\alpha}$, with $+$ ($-$) for sites in the same (opposite) sublattice.

n	$ t_{\alpha\alpha} $	$V_{\alpha\beta}$	$J_{\alpha\alpha}$	$J_{\alpha,-\alpha}$
0	0	21.2	0	0
1	0.384	16.9	5.09	-4.93
2	0.005	16.7	1.11	1.02
3	0.447	15.6	0.52	-0.51
4	0.162	12.6	0.25	-0.18
5	0.084	11.58	0.16	0.12
6	0.007	9.68	0.09	0.08

numerical precision. That includes the on site exchange (Hund's coupling), which is zero due to the orthogonality between same site Wannier spinors [15,39]. From now on, we define the *only* nonzero combination $J_{\alpha\alpha,\beta\beta} \equiv J_{\alpha\beta}$.

The numerical values of the hopping energy, Coulomb interaction and the exchange interaction for n th NNs, is shown in Table I, which is the second main result of the Letter. We find the on site Hubbard $U_{\alpha\beta} \equiv V_{\alpha\beta}(0) = 21.2$ meV, which is much larger than the first NN hopping $t(1)$, and hence the ratio $U/t(1) \sim 55$ falls comfortably in the realm of the Mott regime.

The exchange interaction for first NN sites ($n = 1$) is $|J_{\alpha\beta}(1)| \approx 5$ meV. In general, the diagonal terms $J_{\alpha\alpha}(n) > 0$ are positive definite, whereas the off diagonal ones can be either positive or negative, $J_{\alpha,-\alpha}(n) \approx \pm J_{\alpha\alpha}(n)$, with $+$ ($-$) for i, j sites in the same (opposite) sublattice, as shown in Table I. For sites in the same sublattice, the fact that $J_{\alpha\beta}(n) \approx J_{\alpha\alpha}(n) > 0$ is the same for all four combinations of $\alpha, \beta = \pm$ indexes hints at an emergent $SU(4)$ symmetry between spin and orbital degrees of freedom at quarter filling. For sites in opposite sublattices, the exchange interaction has $SU(2)$ symmetry in the spin. It has also both ferro ($J_{\alpha\alpha} > 0$) and antiferromagnetic ($J_{\alpha,-\alpha} < 0$) correlations in the orbital sector, depending on the orientation of the pseudospins.

Since Hund's coupling is zero, at quarter filling the lower flat bands are in the unitary limit [40], with each moiré superlattice site \mathbf{R}_j being singly occupied and having a well-defined spin σ and orbital quantum number $\alpha = \pm$. Mapping the exchange term in terms of spin $\mathbf{S}_i = \frac{1}{2} d_{\alpha,\sigma}^\dagger(\mathbf{R}_i) \vec{\sigma}_{\sigma\sigma'} d_{\alpha,\sigma'}(\mathbf{R}_i)$ and pseudospin $\boldsymbol{\tau}_i = \frac{1}{2} d_{\alpha,\sigma}^\dagger(\mathbf{R}_i) \vec{\sigma}_{\alpha\beta} d_{\beta,\sigma}(\mathbf{R}_i)$ operators, the result is the ferromagnetic exchange interaction announced in Eq. (1), with $J_{ij} \equiv J_{\alpha\alpha}(n) > 0$ [41]. This Hamiltonian favors ferromagnetic alignment of the spins at zero temperature ($T = 0$). In the orbital sector different states are possible, including canted magnetism with ferromagnetic order in the pseudospin τ^z component, accompanied by staggered (antiferromagnetic) order in the transverse, $\boldsymbol{\tau}^\perp$ direction [42].

The superexchange interaction follows from second order perturbation theory in the hopping energy [43,44] and has the same form as the exchange term in Eq. (1) for $\eta_{ij} = -1$ [15]. The superexchange term has $SU(4)$ symmetry and favors antiferromagnetic alignment between nearest neighbor sites due to Pauli principle. Its coupling $J \rightarrow -t^2/U \approx -0.01$ meV is very small compared to the exchange one, and can be safely ignored.

Ferromagnetic Mott state.—Mott-Hubbard insulators have strongly localized states and are known to be overwhelmingly antiferromagnetic due to strong superexchange interactions ($t^2/U \gg J$) [45–47]. Ferromagnetism occurs mostly either in metallic systems or in metallic bands hybridized with localized moments via the Anderson impurity mechanism [45,46,48]. Within the Hubbard model framework, the only credible mechanism for spin ferromagnetism exists for multiorbital systems in the context of the Kugel-Khomskii model [43,47], where superexchange can become effectively ferromagnetic in the presence of staggered orbital ordering.

We conjecture that the flat bands in twisted graphene bilayers are in a way intermediate between ferromagnetic bad metals and antiferromagnetic Mott-Hubbard insulators. Due to the exotic shape of the Wannier orbitals, the hierarchy between hopping, direct exchange and the local Hubbard interaction, $t \ll J \ll U$, leads to an anomalously small superexchange.

In spite of the fact that U/t is large, the strong overlap between the orbitals found in the noninteracting theory suggests that the system is potentially close to an insulator-metal transition [1] due to a charge fluctuation mechanism, which presently is not well understood [30,31]. Nevertheless, the form of the effective spin Hamiltonian [Eq. (1)] should not depend on the details of this mechanism, as long as the system remains quarter filled and does not undergo a charge-ordering transition (potentially accompanied by dimerization) due to Coulomb interactions. In carbon lattices, which are notoriously stiff [49], charge density wave instabilities are hindered by the high elastic energy cost for the system to deform the lattice and restore charge neutrality.

Interactions should increase the spread of the maximally localized Wannier orbitals, making the system more metallic [31]. In the absence of charge order, the dressed Wannier functions should preserve the symmetries of the lattice and renormalize the couplings U , J , and the hopping t . In that regard, Table I provides an *upper* bound for the Hubbard U coupling, and a *lower* bound for the exchange interaction J and t [50].

Experimental signatures.—Since the honeycomb superlattice is not frustrated, it will exhibit ferromagnetic spin order at $T = 0$ in the universality class of the ferromagnetic (spin S) Heisenberg model. It is well known that the magnetization M , correlation length ξ and the spin susceptibility χ exhibit peculiar features in two dimensions, since for any $T \neq 0$ the system is disordered, with zero

Curie temperature. The model has been extensively studied both in zero and finite external magnetic field H on various lattices [51–54]. At finite field $H \neq 0$, $M(H)$ is finite and strongly temperature dependent. In the regime $T/J \ll 1$, which can take place for $T \approx 2$ K (where $T/J \approx 1/25$), a weak magnetic field of $H \approx 0.2$ T (i.e., $H/J \approx 1/250$) already provides nearly maximum magnetization [52,53]. The spin susceptibility $\chi(H)$ is zero for $T = 0$ and $H \neq 0$ and exhibits a characteristic finite-temperature peak at $T = T_\chi$ which scales in a well-defined way with external field.

It has been established experimentally that doping away from the Mott insulating phase leads to metallic (and even superconducting) behavior [3,4]. A profound new feature has emerged at finite magnetic field, which persists both in weak (Shubnikov–de Haas oscillations) and strong field limits (quantum Hall effect), for hole doping [3,4]. Those measurements suggest a small Fermi surface that develops from doping the correlated insulating phase, accompanied by a possible symmetry breaking of yet unknown origin. The resulting state has a fermionic degeneracy of 2, indicating a reduction of the original fourfold band degeneracy by a factor of 2.

This behavior is consistent with the system being in the proximity to a ferromagnetic Mott state, in which the spins align when nudged by an infinitesimally weak field. At the same time, any long-range order in the orbital sector is expected to be much more fragile and disappear quickly due to charge disorder and the motion of holes in the metallic state. Therefore we conjecture that, in the weak field limit, the ground state emerging from doping the ferromagnetic insulator would be a ferromagnetic, spin-polarized, strongly correlated metal, with the orbital pseudospin symmetry preserved.

B.U. acknowledges P. Jarillo-Harillo, T. Senthil, K. Beach, and O. Vafek for discussions. K.S. and B.U. acknowledge NSF CAREER Grant No. DMR-1352604 for support.

Note added.—After submission of the manuscript we became aware of Ref. [56], which identified a distinct ferromagnetic ground state at quarter filling using different methods. That work does not predict the existence of a spin ferromagnet, in contrast to ours, resulting in a very different physical picture and experimental signatures [55].

*uchoa@ou.edu

- [1] M. Imada, A. Fujimori, and Y. Tokura, *Rev. Mod. Phys.* **70**, 1039 (1998).
- [2] A. Auerbach, *Interacting Electrons and Quantum Magnetism* (Springer-Verlag, New York, 1998).
- [3] Y. Cao, V. Fatemi, S. Fang, K. Watanabe, T. Taniguchi, E. Kaxiras, and P. Jarillo-Herrero, *Nature (London)* **556**, 80 (2018).
- [4] Y. Cao, V. Fatemi, S. Fang, K. Watanabe, T. Taniguchi, E. Kaxiras, and P. Jarillo-Herrero, *Nature (London)* **556**, 43 (2018).
- [5] M. Yankowitz, S. Chen, H. Polshyn, Y. Zhang, K. Watanabe, T. Taniguchi, D. Graf, A. F. Young, and C. R. Dean, *arXiv:1808.07865*.
- [6] A. H. C. Neto, F. Guinea, N. M. R. Peres, K. S. Novoselov, and A. K. Geim, *Rev. Mod. Phys.* **81**, 109 (2009).
- [7] H. C. Po, L. Zou, A. Vishwanath, and T. Senthil, *Phys. Rev. X* **8**, 031089 (2018).
- [8] B. Padhi, C. Setty, and P. W. Phillips, *Nano Lett.* **18**, 6175 (2018).
- [9] X. Y. Xu, K. T. Law, and P. A. Lee, *Phys. Rev. B* **98**, 121406(R) (2018).
- [10] V. Y. Irkhin and Y. N. Skryabin, *JETP Lett.* **107**, 651 (2018).
- [11] A. Thomson, S. Chatterjee, S. Sachdev, and M. S. Scheurer, *Phys. Rev. B* **98**, 075109 (2018).
- [12] J. F. Dodaro, S. A. Kivelson, Y. Schattner, X.-Q. Sun, and C. Wang, *Phys. Rev. B* **98**, 075154 (2018).
- [13] J. M. B. L. dos Santos, N. M. R. Peres, and A. H. C. Neto, *Phys. Rev. Lett.* **99**, 256802 (2007).
- [14] R. Bistritzer and A. H. MacDonald, *Proc. Natl. Acad. Sci. U.S.A.* **108**, 12233 (2011).
- [15] B. Uchoa, V. N. Kotov, and M. Kindermann, *Phys. Rev. B* **91**, 121412(R) (2015).
- [16] X. Dou, V. N. Kotov, and B. Uchoa, *Sci. Rep.* **6**, 31737 (2016).
- [17] C. Xu and L. Balents, *Phys. Rev. Lett.* **121**, 087001 (2018).
- [18] M. O. Goerbig, *Rev. Mod. Phys.* **83**, 1193 (2011).
- [19] A. F. Young, C. R. Dean, L. Wang, H. Ren, P. Cadden-Zimansky, K. Watanabe, T. Taniguchi, J. Hone, K. L. Shepard, and P. Kim, *Nat. Phys.* **8**, 550 (2012).
- [20] A. F. Young, J. D. Sanchez-Yamagishi, B. Hunt, S. H. Choi, K. Watanabe, T. Taniguchi, R. C. Ashoori, and P. Jarillo-Herrero, *Nature (London)* **505**, 528 (2014).
- [21] K. Nomura and A. H. MacDonald, *Phys. Rev. Lett.* **96**, 256602 (2006).
- [22] J. Alicea and M. P. A. Fisher, *Phys. Rev. B* **74**, 075422 (2006).
- [23] D. A. Abanin, B. E. Feldman, A. Yacoby, and B. I. Halperin, *Phys. Rev. B* **88**, 115407 (2013).
- [24] I. Sodemann and A. H. MacDonald, *Phys. Rev. Lett.* **112**, 126804 (2014).
- [25] B. Huang *et al.*, *Nature (London)* **546**, 270 (2017).
- [26] W. B. Yelon and R. Silbergliitt, *Phys. Rev. B* **4**, 2280 (1971).
- [27] E. J. Samuelsen, R. Silbergliitt, G. Shirane, and J. P. Remeika, *Phys. Rev. B* **3**, 157 (1971).
- [28] A. S. Erickson, S. Misra, G. J. Miller, R. R. Gupta, Z. Schlesinger, W. A. Harrison, J. M. Kim, and I. R. Fisher, *Phys. Rev. Lett.* **99**, 016404 (2007).
- [29] K. I. Kugel and D. Khomskii, *Sov. Phys. JETP* **37**, 725 (1973).
- [30] J. M. Pizarro, M. J. Calderon, and E. Bascones, *arXiv:1805.07303*.
- [31] F. Guinea and N. R. Walet, *Proc. Natl. Acad. Sci. U.S.A.* **115**, 13174 (2018).
- [32] The functions $V_\sigma(\mathbf{r}) = V_{pp\sigma}^0 \exp[-(|\mathbf{r}| - d)/\lambda]$ and $V_\pi(\mathbf{r}) = V_{pp\pi}^0 \exp[-(|\mathbf{r}| - a/\sqrt{3})/\lambda]$, with $d = 3.35$ Å the interlayer distance, $a = 2.42$ Å in in-plane lattice constant, $V_{pp\sigma}^0 = 0.39$ eV, $V_{pp\pi}^0 = -3.09$ eV, and $\lambda = 0.27$ Å. See Ref. [33].

- [33] X. Lin and D. Tománek, *Phys. Rev. B* **98**, 081410(R) (2018).
- [34] M. S. Tang, C. Z. Wang, C. T. Chan, and K. M. Ho, *Phys. Rev. B* **53**, 979 (1996).
- [35] H. C. Po, H. Watanabe, and A. Vishwanath, *Phys. Rev. Lett.* **121**, 126402 (2018).
- [36] A. A. Mostofi, J. R. Yates, G. Pizzi, Y.-S. Lee, I. Souza, D. Vanderbilt, and N. Marzari, *Comput. Phys. Commun.* **185**, 2309 (2014).
- [37] J. Kang and O. Vafek, *Phys. Rev. X* **8**, 031088 (2018).
- [38] N. F. Q. Yuan and L. Fu, *Phys. Rev. B* **98**, 045103 (2018).
- [39] M. Koshino, N. F. Q. Yuan, T. Koretsune, M. Ochi, K. Kuroki, and L. Fu, *Phys. Rev. X* **8**, 031087 (2018).
- [40] B. Coqblin and A. Blandin, *Adv. Phys.* **17**, 281 (1968).
- [41] See Supplemental Material at <http://link.aps.org/supplemental/10.1103/PhysRevLett.122.246402> for details.
- [42] In the absence of the long range part of the Coulomb interaction, twisted graphene bilayers may stabilize a spiral state in the moiré superlattice. See L. A. Gonzalez-Arraga, J. L. Lado, F. Guinea, and P. San-Jose, *Phys. Rev. Lett.* **119**, 107201 (2017).
- [43] K. I. Kugel and D. I. Khomskii, *Sov. Phys. Usp.* **25**, 231 (1982).
- [44] J. W. F. Venderbos and R. M. Fernandes, *Phys. Rev. B* **98**, 245103 (2018).
- [45] P. W. Anderson, Theory of Magnetic Exchange Interactions: Exchange in Insulators and Semiconductors, in *Solid State Physics*, edited by F. Seitz and D. Turn-bull (Academic Press, 1963), Vol. 14, pp. 99–214.
- [46] P. W. Anderson, *Phys. Rev.* **115**, 2 (1959).
- [47] D. I. Khomskii, *Basic Aspects of the Quantum Theory of Solids* (Cambridge University Press, Cambridge, England, 2010).
- [48] T. Moriya, *Spin Fluctuations in Itinerant Electron Magnetism* (Springer-Verlag, Berlin Heidelberg, 1985).
- [49] J.-U. Lee, D. Yoon, and H. Cheong, *Nano Lett.* **12**, 4444 (2012).
- [50] Experimental evidence of a sizeable Mott gap indicates that the ratio U/t will remain large even if charging effects are explicitly taken into account. In the scenario where strong charging effects halve the local Coulomb energy U and double the bandwidth of the flat bands (therefore doubling t), the exchange interaction J will still be at least one order of magnitude larger than the superexchange, while J itself should increase. Hence, Table I gives a *conservative* estimate for the spin exchange interaction entering in Hamiltonian [Eq. (1)].
- [51] P. Kopietz and S. Chakravarty, *Phys. Rev. B* **40**, 4858 (1989).
- [52] T. N. Antsygina, M. I. Poltavskaya, I. I. Poltavsky, and K. A. Chishko, *Phys. Rev. B* **77**, 024407 (2008).
- [53] I. J. Junger, D. Ihle, L. Bogacz, and W. Janke, *Phys. Rev. B* **77**, 174411 (2008).
- [54] At low $T \ll J$, the zero-field susceptibility exhibits characteristic 2D deviation from the conventional Curie-Weiss law, $T\chi \sim (T/J)^3 \exp(2cJ/T)$, while the magnetization is zero at any finite T .
- [55] Our results contrast with those of Ref. [56], where a ferromagnetic state with maximal spin-valley entanglement and zero net magnetic moment per particle is found at quarter filling. We show from the actual spin exchange Hamiltonian of the problem that the ground state is a product state between spin and orbital sectors with maximum magnetic moment per site. This significant difference in physical results seems to originate from their approach to truncate the range of interactions, coupled with a variational treatment of the ground state wave function. By contrast, our mapping of Coulomb interactions, via Eqs. (9) and (10), into the effective spin exchange Hamiltonian [Eq. (1)] is *exact* and leads to the prediction of a unique spin-polarized ferromagnetic ground state.
- [56] J. Kang and O. Vafek, preceding Letter, *Phys. Rev. Lett.* **122**, 246401 (2019).